energies

MDPI

Article

Study on Influential Mechanism of Trailing Edge Sweep Angle on Aerodynamic Noise of a Centrifugal Air Compressor

Shizhong Sun [1], Yiwei Feng [1], Ziwen Xing [1], Minglong Zhou [2], Wenqing Chen [2], Chuang Wang [1,*] and Hanyang Cui [1]

[1] School of Energy and Power Engineering, Xi'an Jiaotong University, Xi'an 710049, China
[2] Suzhou Academy, Xi'an Jiaotong University, Suzhou 215123, China
* Correspondence: chuangwang@xjtu.edu.cn; Tel.: +86-13289227655

Abstract: As the main noise source in the hydrogen fuel cell system, the noise level of the centrifugal air compressor greatly affects the comfort of the hydrogen fuel cell vehicle, and can be effectively reduced by optimizing the trailing edge sweep angle of the blade. In this paper, the computational fluid dynamics model was used to study the influence of the trailing edge sweep angle on the aerodynamic performance and flow characteristics of a centrifugal air compressor for vehicle fuel cells. The Ffowcs Williams–Hawkings equation and the computational fluid dynamics–boundary element coupling method were adopted to calculate the dipole source strength on the surface of the blade and the radiated aerodynamic noise, respectively, under the different trailing edge sweep angles. The results showed that the trailing edge sweep could lead to an increase in pressure ratio as well as isentropic efficiency, and a decrease in the intensity of flow separation. Meanwhile, the sound pressure level of the compressor under each working condition could be effectively reduced by the trailing edge sweep. When the rotation speed was 80,000 r·min^{-1} and the blade trailing edge sweep angle was 15°, the sound pressure level of the radiated aerodynamic noise was 5.8 dBA lower than that without sweep.

Keywords: fuel cell; centrifugal air compressor; aerodynamic noise; CFD-BEM coupling method; trailing edge sweep

Citation: Sun, S.; Feng, Y.; Xing, Z.; Zhou, M.; Chen, W.; Wang, C.; Cui, H. Study on Influential Mechanism of Trailing Edge Sweep Angle on Aerodynamic Noise of a Centrifugal Air Compressor. *Energies* **2022**, *15*, 7410. https://doi.org/10.3390/en15197410

Academic Editor: Alessandro Bianchini

Received: 12 September 2022
Accepted: 29 September 2022
Published: 9 October 2022

1. Introduction

Hydrogen fuel cell vehicles have developed as the leading research focuses of new energy vehicles for the advantages of clean and high efficiency. As the main noise source in the hydrogen fuel cell system, the noise level of the centrifugal air compressor greatly affects the comfort of the hydrogen fuel cell vehicle. Further, aerodynamic noise is the main noise source of centrifugal air compressors, and numerous studies have been conducted on this subject.

Raitor et al. [1] decomposed the aerodynamic noise into blade tip clearance noise, discrete single-tone noise (blade passage frequency and its harmonics), "buzz-saw" noise (rotation frequency and its harmonics), and broadband noise. Subsequently, many studies have been conducted on the aerodynamic noise of centrifugal compressors. The FW–H (Ffowcs Williams–Hawkings) equations [2,3], the broadband noise method [4], and the CFD (Computational Fluid Dynamics)-BEM (Boundary Element Method) coupling method [5,6], are used for simulation of the aerodynamic noise.

In terms of blade shape optimization and channel modification, a lot of research has investigated the sweep shapes of the leading edge (LE) and trailing edge (TE) of impellers. Ganesh et al. [7] studied the effects of different sweep angles of the LE on the aerodynamic performance of impellers, and the results showed that there were different optimal sweep angles for different highest aerodynamic performances. Zhao et al. [8] studied the influence of the four different types of LE sweep on aerodynamic performance. They found the

pressure ratio (*PR*), isentropic efficiency (η_{is}), and stall margin of transonic impellers could be improved by tip-forward sweep of LE. Guo et al. [9] investigated the forward sweep of LE on the flow characteristics of a transonic centrifugal compressor, and the results showed that the hybrid sweep of LE could expand the stall margin and improve the *PR* and η_{is}. Wang et al. [10] chose the impeller inlet inclination as one of the optimization variables when optimizing the impeller, and reduced the impeller inlet inclination to improve impeller efficiency. Tian et al. [11] found that the TE free-form sweep expanded the stall margin of the transonic centrifugal compressor impeller, suppressed the combination of the clearance flow at TE with the main flow, and improved the *PR* and η_{is}. Tian et al. [12] also studied the effect of a sweep angle of 15° on the impeller aerodynamic performance, and the results showed that the application of TE sweep can also increase the efficiency of the impeller compared with free-form sweep. Since the TE sweep affects the internal flow characteristics of the impeller, which will further affect the aerodynamic noise, it is necessary to study the effect of the TE sweep on the aerodynamic noise excitation and radiation of the impeller. In addition, previous studies have investigated the effect of the TE sweep angle (α_{TE}) on impeller performance at a fixed α_{TE}, but have not explored the influence of α_{TE} on the aerodynamic performance and acoustic characteristics of the impeller.

Based on the previous research, this paper investigates the aerodynamic performance and flow characteristics of a centrifugal air compressor for vehicle fuel cell systems. The influence of α_{TE} on aerodynamic performance and flow characteristics is studied by the CFD method. The FW–H equation and the CFD–BEM coupling method are used to explore the effect of the α_{TE} on the excitation and radiation of the aerodynamic noise.

2. Numerical Method

The object of the paper is a centrifugal air compressor for fuel cells. The impellers are semi-open without splitters and the diffuser is bladeless. The main parameters of impellers are shown in Table 1.

Table 1. Main parameters of the impeller.

Parameter	Value	Parameter	Value
Rated speed/r·min^{-1}	80,000	Inlet diameter/mm	42.86
Design mass flow/kg·s^{-1}	0.12	Outlet diameter/mm	80
Design pressure ratio	1.7	Leading edge sweep angle/°	15
Blade number	13	Blade outlet angle/°	57
Heights of the tip clearance/mm	0.18		

The blade-trailing edge sweep angle is defined as the inclination angle of the blade trailing-edge tip along the flow direction in the meridian flow path. Figure 1 shows the meridian flow path and the α_{TE} of the impeller. The TE of the original impeller is with no sweep. Combining the trial calculation and the consideration of impeller structural strength, parameters α_{TE} of 10/15/20/25/30° were selected to study.

The inlet state of the air compressor is at atmospheric pressure, and the main parameters of the three operating conditions are shown in Table 2.

Table 2. Main parameters of operating conditions.

	Idle Condition (IC)	Common Condition (CC)	High-Speed Condition (HC)
Rotation speed [r·min^{-1}]	30,000	72,000	80,000
Mass flow [g·s^{-1}]	48.0	107.2	120.8

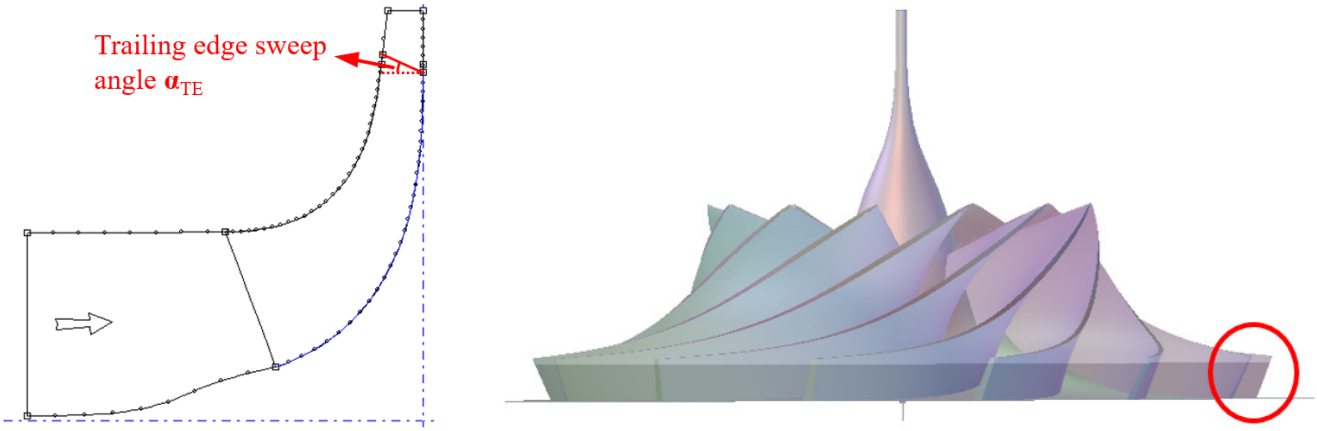

Figure 1. Schematic diagram of impeller meridian flow path and α_{TE}.

2.1. Introduction of the CFD Model

In this paper, the impeller mesh was generated by Turbogrid. ANSYS CFX was used to numerically solve the three-dimensional Reynolds-averaged Navier–Stokes equations (RANS) to simulate the aerodynamic performance and flow characteristics of the impeller.

The flow and heat transfer of fluids conform to the laws of conservation of physics, which include the law of conservation of mass, the law of conservation of momentum, and the law of energy conservation. Since the flow in twin-screw refrigeration compressors is in a turbulent motion state, the system also needs to comply with the additional turbulent transport equation. The governing equations are mathematical descriptions of these conservation laws.

Any flow problem must satisfy the law of conservation of mass, which means that the mass added to the fluid microelement in unit time is equal to the net mass flowing into the microelement at the same time. According to this law, a general form of mass conservation equation can be obtained, which is applicable to compressible flow and incompressible flow. The source term S_m can be any custom source term:

$$\frac{\partial \rho}{\partial t} + \frac{\partial(\rho u)}{\partial x} + \frac{\partial(\rho v)}{\partial y} + \frac{\partial(\rho w)}{\partial z} = S_m \tag{1}$$

The law of conservation of momentum is also a law that must be satisfied by any flow system. The change rate of the momentum of a fluid in a microelement to time is equal to the sum of forces acting on the microelement:

$$\begin{cases} \frac{\partial(\rho u)}{\partial t} + \mathrm{div}\left(\rho u \vec{U}\right) = div(\eta \cdot \mathrm{grad} u) + S_u - \frac{\partial p}{\partial x} \\ \frac{\partial(\rho v)}{\partial t} + \mathrm{div}\left(\rho v \vec{U}\right) = div(\eta \cdot \mathrm{grad} v) + S_v - \frac{\partial p}{\partial y} \\ \frac{\partial(\rho w)}{\partial t} + \mathrm{div}\left(\rho w \vec{U}\right) = div(\eta \cdot \mathrm{grad} w) + S_w - \frac{\partial p}{\partial z} \end{cases} \tag{2}$$

A flow system containing heat exchange must also satisfy the law of conservation of energy, which is the necessary equation for obtaining the temperature field of the fluid. The increase rate of energy in the microelement is equal to the net heat flow into the microelement plus the work done by the volume force and surface force on the microelement. The essence of this law is the first law of thermodynamics:

$$\frac{\partial(\rho T)}{\partial t} + \mathrm{div}\left(\rho T \vec{U}\right) = \mathrm{div}\left(\frac{k}{c_p}\mathrm{grad} T\right) + S_T \tag{3}$$

Since the flow is in a turbulent motion state in twin-screw refrigeration compressors, the system also needs to comply with the additional turbulent transport equation. This paper used the Shear Stress Transport model. The shear stress transport (SST) model is improved by the standard k-ω model, which combines the advantages of the k-ω model in the near-wall region calculation and the advantages of the k-ε model in the far-field calculation; as a result, it is more accurate and reliable for a wider class of flows than the standard k-ω model [13,14]:

$$\begin{cases} \frac{\partial(\rho k)}{\partial t} + \frac{\partial(\rho k u_i)}{\partial x_i} = \frac{\partial}{\partial x_j}\left(\Gamma_k \frac{\partial k}{\partial x_j}\right) + G_k - Y_k + S_k \\ \frac{\partial(\rho \omega)}{\partial t} + \frac{\partial(\rho \omega u_i)}{\partial x_i} = \frac{\partial}{\partial x_j}\left(\Gamma_\omega \frac{\partial \omega}{\partial x_j}\right) + G_\omega - Y_\omega + D_\omega + S_\omega \end{cases} \quad (4)$$

The model includes the impeller inlet extension, the single channel, and the outlet extension. The PR and η_{is} are used as the criterion for grid independence verification. The pressure ratio of the compressor is calculated as:

$$PR = P_{out}/P_{in} \quad (5)$$

where the P_{out} is the total pressure of the outlet and P_{in} is the total pressure of the inlet. The isentropic efficiency is calculated as:

$$\eta_{is} = \frac{PR^{\frac{k-1}{k}} - 1}{\frac{T_{out}}{T_{in}} - 1} \quad (6)$$

where k is the specific heat ratio of air, T_{out} is the temperature of the outlet, and T_{in} is the temperature of the inlet. Six sets of grids with different element numbers were plotted, and the curves of calculation results are plotted in Figure 2. It can be seen from Figure 2 that when the number of elements is greater than 453,235, the mass flow calculation difference is less than 0.5%, so the number of elements is selected as 453,235 in this study.

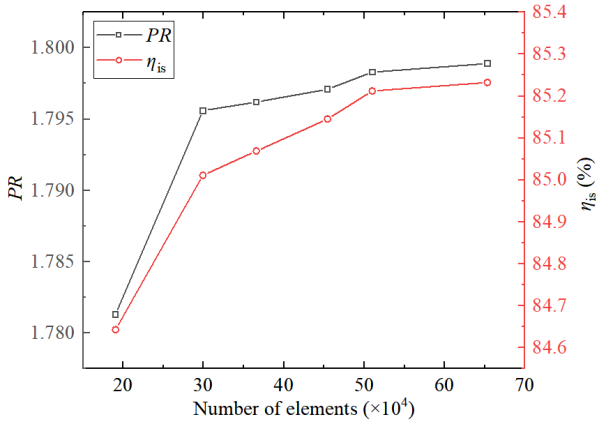

Figure 2. Grid independence verification.

The boundary condition of the inlet is set to a total pressure of 101.3 kPa, and a total temperature of 293.15 K. The outlet boundary condition is set to mass flow outlet, with periodic boundary conditions on both sides of the blade, and adiabatic non-slip boundary on all walls. The calculation is considered converged when the calculated residuals are reduced to below 10^{-6} and the relative error of the inlet and outlet mass flow is less than 0.5%.

2.2. CFD–BEM Coupling Model

A CFD–BEM-coupled aerodynamic acoustic calculation model is established to study the aerodynamic noise induction mechanism. The schematic diagrams of the aerodynamic noise calculation model are shown in Figure 3. The acoustic calculation is to obtain the

solution of the Helmholtz equation satisfying acoustic boundary conditions through the numerical solution. The model is composed of a rotating dipole sound source, the acoustic boundary element mesh, and the field point. In terms of the sound source, the RANS method is applied to calculate the unsteady flow of the compressor, and the time domain fluctuating pressure on the impeller surface is set as the acoustic excitation source through the boundary conditions for aeroacoustic calculation. The acoustic boundary element grid is composed of the inner wall of the flow channel formed by the diffuser and volute. The inlet boundary is set as the opening and the outlet of the volute is set as the non-reflecting boundary. Field points include acoustic monitoring points at the inlet and outlet of the acoustic model and acoustic directional points. Field points SP1 and SP2 are set 20 mm away from the volute inlet and outlet to monitor the near-field noise radiated. Acoustic directional field points are set on the plane composed of the inlet and outlet axes. Twelve field points are evenly distributed on the circumference with the center of the inlet section of the centrifuge as the center and a radius of 1 m to study the sound pressure directivity during the outward radiation of the noise.

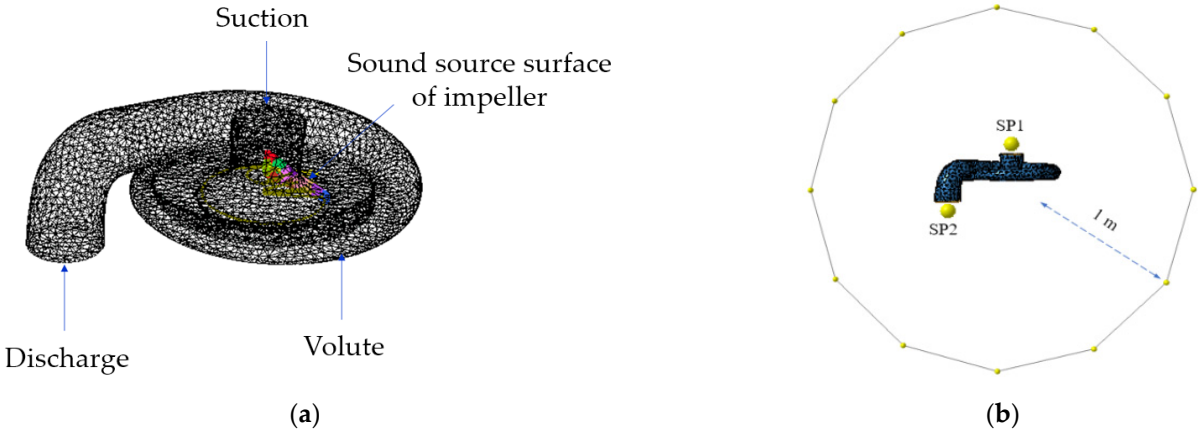

Figure 3. Schematic diagrams of the aerodynamic noise calculation model: (**a**) acoustic model; (**b**) field points of acoustic model.

According to the time domain sampling method in the Nyquist sampling theorem, the maximum frequency allowed by the acoustic model can be calculated when the time step of the unsteady CFD calculation is greater than 100 kHz, which far exceeds the maximum frequency of 20 kHz of humanly audible sounds, meeting the requirements of computational analysis. The maximum calculation frequency of the acoustic model is set to 14 times the impeller rotational fundamental frequency, and the calculation range includes the first-order blade passing frequency with a frequency resolution of 1/10 of the impeller rotational fundamental frequency. In accordance with the basic assumptions of acoustic calculation, at least 6 acoustic units are ensured in the minimum wavelength range, and the maximum side length of the acoustic unit is set according to the maximum calculation frequency required at the corresponding speed under different operating conditions.

2.3. Numerical Model Validation

In order to verify the validity of the numerical calculation method in this paper, the aerodynamic performance of the centrifugal air compressor for fuel cells is tested by a compressor test rig. Thermal performance such as mass flow rate, *PR*, power consumption, etc. is tested by the vehicle fuel cell air compressor performance test rig. The inlet port of the air compressor is connected to an air filter. The outlet of the air compressor is connected to a flow meter, an air buffer tank, a back pressure valve, and sensors. The schematic diagram of the test rig is shown in Figure 4. The CFD calculated *PR* is 1.76, and the error is 0.34% compared with the test result of 1.79. Thus, the model calculation is accurate and reliable.

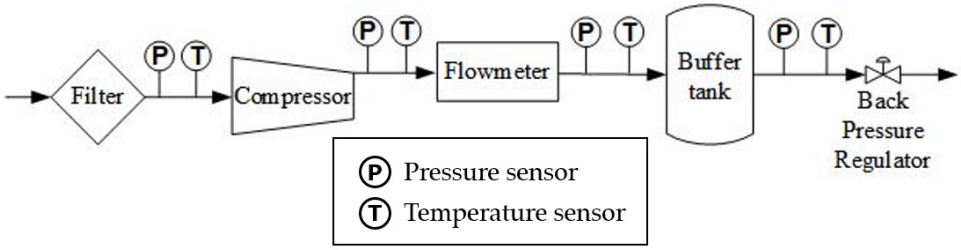

Figure 4. Schematic diagram of the performance test rig of the centrifugal air compressor.

3. Aerodynamic Performance and Flow Characteristics

The flow characteristics are calculated by the CFD to illustrate the influential mechanism of the α_{TE} on the aerodynamic performance.

3.1. Aerodynamic Performance

Figure 5 shows the η_{is} of impellers with different α_{TE}. The η_{is} of the impeller with TE sweep is improved in three working conditions. The higher the speed is, the greater the η_{is} improves. Compared with the non-sweep impeller, the peak η_{is} of the impeller with a sweep angle of 10° is increased by 0.26%, 0.62%, and 0.67%, respectively, at three conditions, while the change of the maximum efficiency line is small. With the adoption of trailing edge sweep, the η_{is} is improved even more in low-efficiency flow conditions, up to 0.83%, which can effectively broaden the working range and improve the stability of the air compressor. As for the effect of sweep angle, in each speed and mass flow rate, the η_{is} is the highest when the sweep angle is 10°, followed by 20°. The efficiency without sweep angle is the lowest. The mass flow rate has little effect on the η_{is}. Accordingly, the flow conditions with peak performance are selected to investigate the effect of α_{TE} on impeller performance and flow characteristics in the following study.

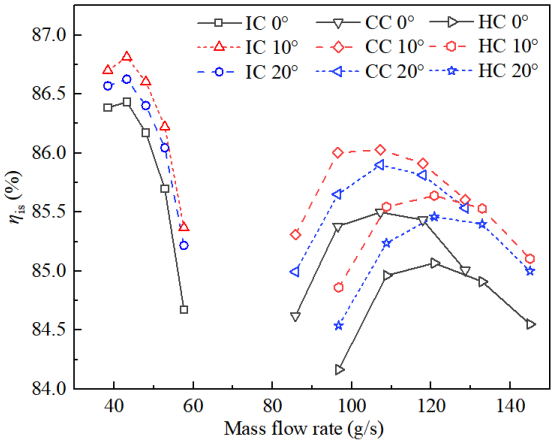

Figure 5. η_{is} under different conditions.

Figure 6 shows the effect of α_{TE} on the performance of the air compressor under flow conditions with peak performance. The TE sweep can effectively increase the work area of the impeller and improve the slip coefficient, thus increasing the *PR*. The larger the α_{TE} is, the higher the *PR* is. The increase in the *PR* is more with higher speed. The η_{is} of the TE with sweep significantly improves compared to that without the sweep. The variation of the η_{is} shows a trend of decreasing first and then increasing. The minimal η_{is} is at the sweep angle of 15°~20°. Increasing the α_{TE} increases the chord length of the blade tip. On the one hand, it increases the work area of the impeller and the overall load; on the other hand, the length of the flow path near the impeller shroud side is increased, further affecting the average load along the flow direction, thereby affecting the flow separation loss in the process.

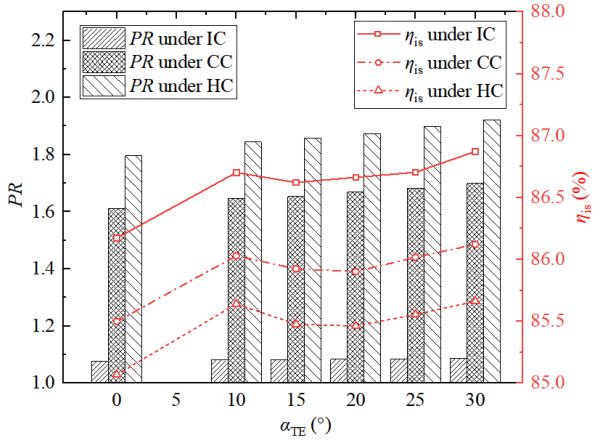

Figure 6. Performance of air compressor with different α_{TE} under peak performance flow condition.

3.2. Flow Characteristics

In order to explore the influential mechanism of α_{TE} on the aerodynamic performance of the air compressor, the flow characteristics of impellers with different α_{TE} are analyzed in the flow condition with the highest efficiency under HC.

Figure 7 shows the static entropy contours at 80% blade height. There are two obvious entropy-increasing regions in the impeller flow passage near the middle of the blade and near the TE. With the TE sweep, the flow loss caused by the mixing of the leakage flow of blade tip clearance flow and the main flow is suppressed. According to the area size of the maximum static entropy area in the figure, the suppression effect is best when the α_{TE} is 10° and 30°. However, the flow separation loss of the pressure side near the TE gradually increases. The TE sweep increases the load near the TE, making the load distribution of the entire impeller passage more uniform. As a result, the flow loss inside the whole impeller is smaller and the flow is smoother with the TE sweep.

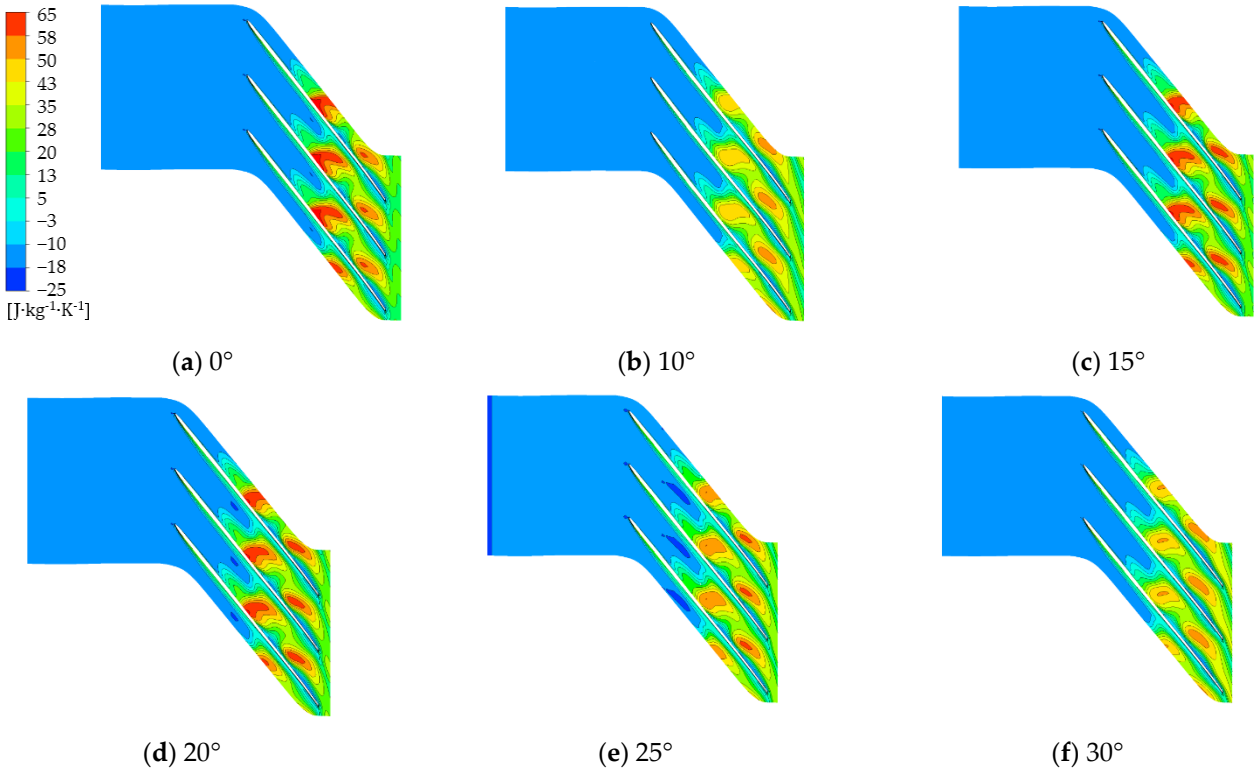

Figure 7. Static entropy contours at 80% blade height with different α_{TE}.

Figure 8 shows the distribution of static entropy at 50% blade height. There is an obvious entropy-increasing region near the suction side of TE. The TE without sweep has stronger flow separation compared with the TE with sweep, and the TE sweep can effectively reduce the intensity of TE flow separation. The suppression effect on the flow separation decreases first and then increases with the increase in α_{TE} by affecting the average load along the flow direction.

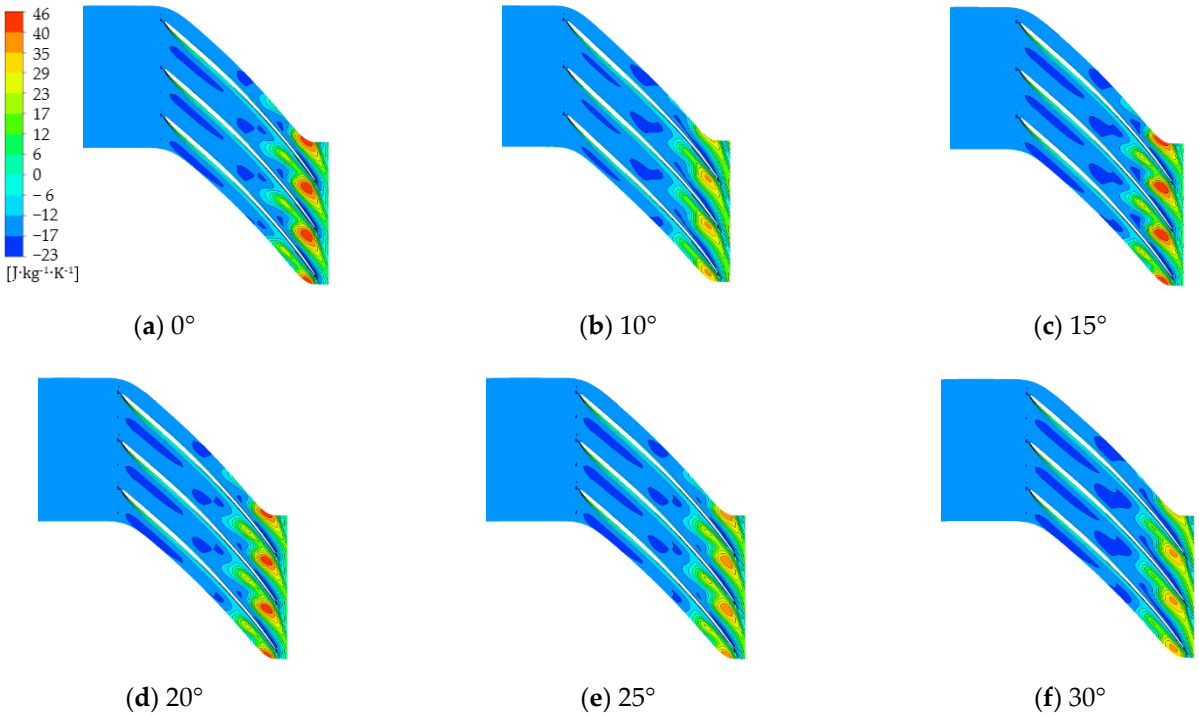

Figure 8. Static entropy contours at 50% blade height with different α_{TE}.

Figure 9 shows the load distribution at 50% blade height with different α_{TE}. The static load at LE is relatively small and is less affected by the TE sweep. The load at TE is relatively large. Enlarging the sweep angle can increase the pressure on the pressure surface and the inlet surface, thereby increasing *PR*. In TE, there exists a region of a sharp increase in Mach number and a sudden decrease in pressure. The increase in the α_{TE} will make the pressure in the low-pressure region lower.

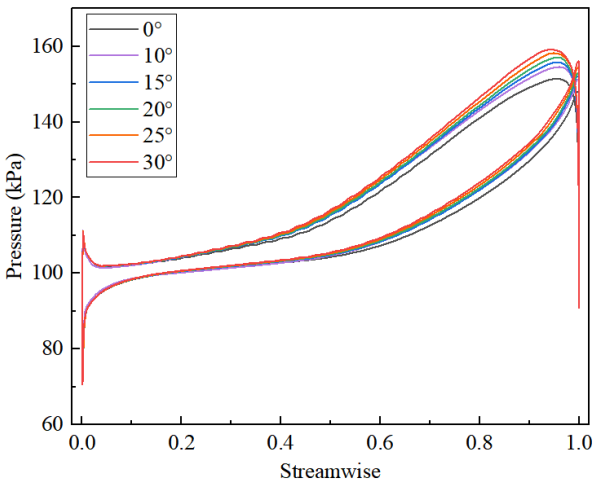

Figure 9. Load distribution at 50% blade height.

The α_{TE} affects the flow loss caused by the mixing between tip clearance flow and main flow, the flow separation loss in the tip near the TE pressure surface, and the flow separation loss at TE of the middle blade height, thus affecting the efficiency of the impeller. The internal flow characteristics of the impeller brought about by α_{TE} will further affect the characteristics of the aerodynamic noise of the compressor.

4. Characteristics of Aerodynamic Noise

The FW–H equations are used to calculate the dipole source strength on the surface of the blade, which is the main excitation source of aerodynamic noise. The CFD–BEM coupling method is used to study the influence of the trailing edge sweep angle on the radiated aerodynamic noise. The influential mechanism of the α_{TE} on the aerodynamic noise is revealed in this section.

4.1. Calculation of Excitation Source Intensity by FW–H Equation

The Ffowcs Williams–Hawkings (FW–H) analogy enables extrapolation of the sound emitted from a simulated flow scenario to the far-field. The idea is to estimate small pressure fluctuations at receiver locations. The equation for pressure is computed as a sum of a monopole term, a dipole term, and a quadrupole term.

$$p'(\overline{x},t) = {p'}_T(\overline{x},t) + {p'}_L(\overline{x},t) + {p'}_Q(\overline{x},t) \tag{7}$$

The monopole source is related to the motion of the source surface and defines the volume displacement of the vibration source. The monopole term is given as follows:

$${p'}_T(\overline{x},t) = \frac{1}{4\pi}\left(\frac{\partial}{\partial t}\int_S \left[\frac{Q}{r(1-M_r)}\right]_{ret} dS\right) \tag{8}$$

with $Q = \rho_0\left[\left(1-\frac{\rho}{\rho_0}\right)v_i + \frac{\rho u_i}{\rho_0}\right]n_i$ where u is fluid velocity, v is control surface velocity, and ρ_0 is far field density.

The dipole source describes the interaction between the fluid and the source surface and defines the load fluctuations applied to the surface. The dipole term is given by:

$$p'_L(\overline{x},t) = \frac{1}{4\pi}\left(-\frac{\partial}{\partial x_i}\int_S \left[\frac{L_i}{r(1-M_r)}\right]_{ret}\right)dS \tag{9}$$

with $L_i = P_{ij}n_i + \rho u_i(u_n - v_n)$ and $P_{ij} = (p-p_0)\delta_{ij} - \sigma_{ij}$. The parameter u_n is the fluid velocity component normal to the surface, n_i is the surface normal vector, σ_{ij} is the viscous stress tensor, P_{ij} is the compressive stress tensor.

The quadrupole source is related to the turbulent pulsation intensity of the fluid. The quadrupole term is:

$$p'_Q(\overline{x},t) = \frac{1}{4\pi}\left(-\frac{\partial^2}{\partial x_i \partial x_j}\int_V \left[\frac{T_{ij}}{r(1-M_r)}\right]_{ret}\right)dV \tag{10}$$

where T_{ij} is the Lighthill stress tensor. The subscript *ret* is short hand for retarded time, and indicates the time of emission. The parameter M_r in the integrand's denominator is the Mach number for the source towards the observer location and where r_i is the distance from the source point to the observer.

Table 3 shows the average intensity of the acoustic pole of the impellers with different α_{TE} under the HC with the maximum efficiency flow condition. The intensity of the monopole source is low, which is less affected by the rotation speed, flow, and α_{TE}. Thus, the monopole source is not the main source of aerodynamic noise, while the quadrupole source increases with the increase in impeller speed and flow. However, the intensity of the quadrupole source is less than 1/9 of that of the dipole source, so the dipole source is chosen for the study.

Table 3. Intensity of acoustic pole under HC [Pa].

α_{TE}	0°	10°	15°	20°	25°	30°
Monopole	153	145	150	158	158	149
Dipole	113,643	112,394	111,928	112,969	113,362	113,374
Quadrupole	11,816	11,692	11,586	11,657	11,587	11,618

Figure 10 shows the dipole source excitation intensity of channel cross sections of impellers with different α_{TE} under HC. The distribution of dipole source excitation intensity in the same blade is similar to the pressure distribution, which gradually increases along the flow direction and reaches a maximum near TE. It can be clearly seen that the intensity of the source excitation along the flow direction generally decreases with the increase in the α_{TE}. The larger the α_{TE} is, the greater the blade area near TE at higher source excitation intensity is. α_{TE} accordingly affects the overall source excitation intensity of the blade. At the same time, either the minimum distance between the blade and the diffuser or the volute are both shorter with larger α_{TE}, and the propagation path of the aerodynamic noise under the blade excitation will be shortened accordingly. Under the effect of several factors, it is necessary to use the CFD–BEM coupling method to calculate the aerodynamic noise, which provides a reference to explore the influence of α_{TE} on the aerodynamic noise of the air compressor in the actual operation.

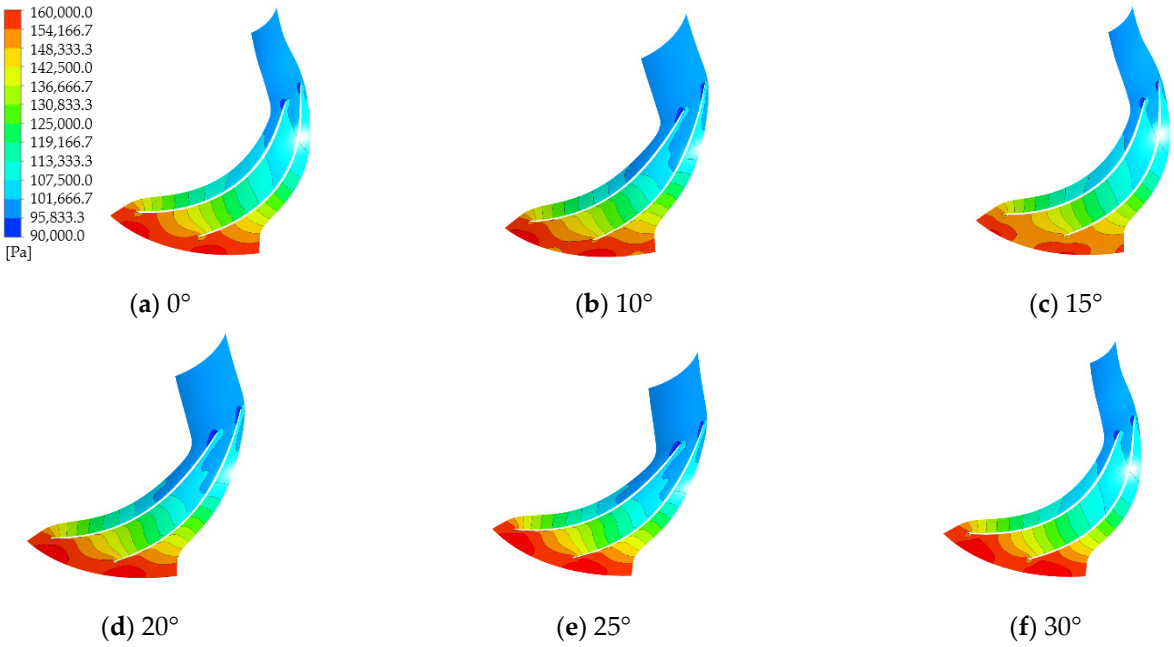

Figure 10. Excitation intensity of acoustic dipole of impellers with different α_{TE}.

4.2. Calculation of Aerodynamic Noise Characteristics by CFD–BEM Coupling Method

Under IC, the blade rotation base frequency of the centrifugal air compressor is 500 Hz, the blade number is 13, and the blade passing frequency is 6500 Hz. The near-field noise spectrum at the inlet of the impeller and outlet of the volute is shown in Figure 11. The spectral characteristics of the volute inlet and outlet are basically the same, the noise at the volute outlet is slightly higher than that at the inlet. The noise mainly includes broadband noise and more prominent, "buzz-saw" noise. The "buzz-saw" noise has a typical periodic harmonic characteristic with a fundamental frequency of 500 Hz, which coincides with the blade rotation fundamental frequency under IC.

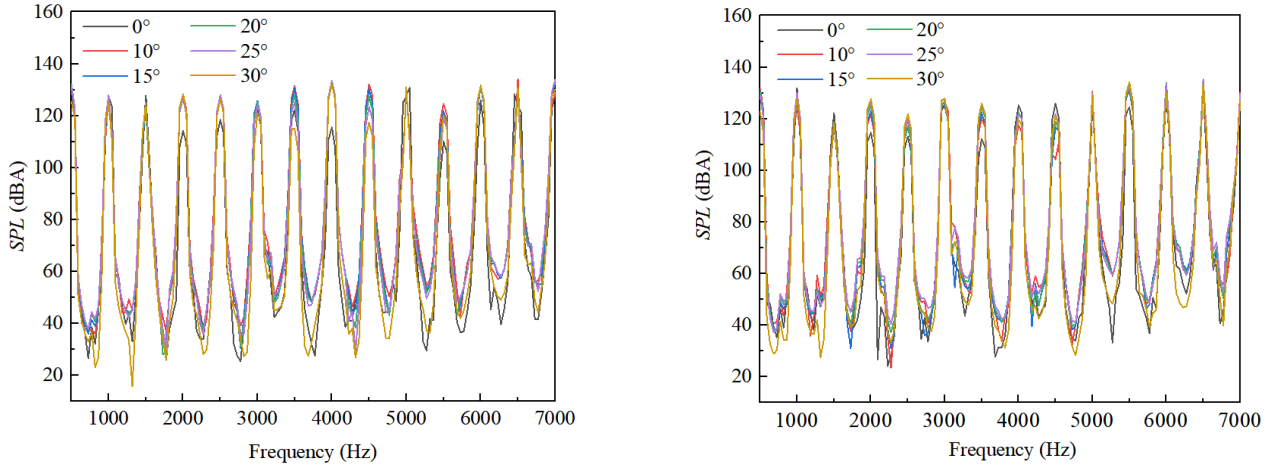

(**a**) Near-surface noise characteristics of the outlet of the volute

(**b**) Near-surface noise characteristics of the inlet of the volute

Figure 11. Noise spectrum characteristics of centrifugal air compressor under IC.

Figure 12 shows the directivity of noise radiation under IC. The noise radiated by the centrifugal air compressor has obvious directivity. Moreover, the noise is relatively higher in the conical area of ±60° of the axis of the inlet and outlet. Due to the high pressure at the TE, the great pressure fluctuation, and the high aerodynamic noise induced during the operation of the compressor, the sound pressure level (*SPL*) radiated from the volute outlet is slightly higher than that of the inlet. Accordingly, the outlet noise has a greater impact on the noise of the compressor. The α_{TE} mainly affects the flow characteristics and acoustic characteristics of the TE and has a greater impact on the volute outlet noise. Therefore, the first four order noise peaks and total *SPL* of the rotational fundamental frequency at the volute outlet are analyzed. The influence mechanism of α_{TE} on the noise is also investigated.

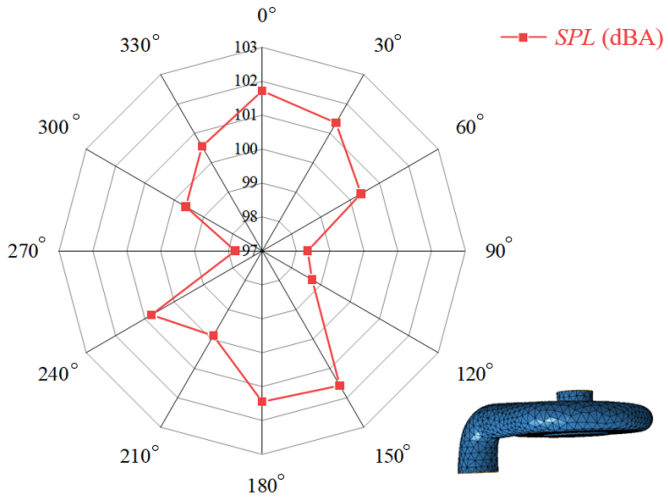

Figure 12. Acoustic directivity under IC.

The total *SPL* of the aerodynamic noise of impellers with different α_{TE} at different operating conditions is shown in Figure 13. Under different conditions, the total *SPL* of aerodynamic noise decreases when adopting sweep compared to TE without sweep. The higher the speed, the more obvious the noise reduction effect. With the increase in α_{TE}, the *SPL* of aerodynamic noise decreases first, then increases, and then decreases due to the influence of impeller sound source intensity, position, and radiation area. The *SPL* is the lowest when the sweep angle is 15°. Compared with no sweep, when α_{TE} is 15°, the *SPL* is

reduced from 134.0 dBA to 132.6 dBA by 1.4 dBA under IC. Under CC, the *SPL* is reduced from 137.9 dBA to 133.6 dBA by 4.3 dBA. Under HC, the *SPL* is reduced from 142.6 dBA to 136.8 dBA by 5.8 dBA.

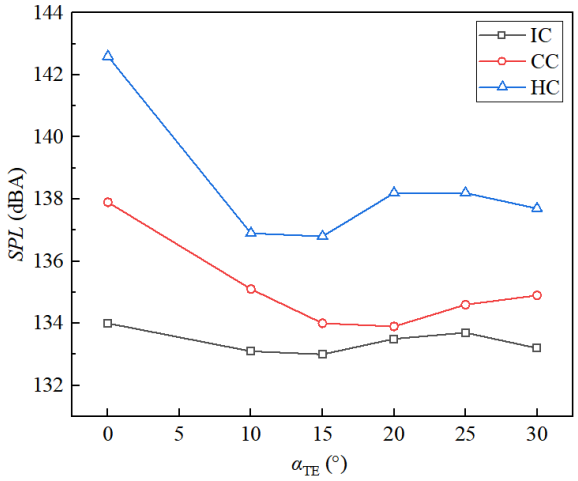

Figure 13. Noise *SPL* at volute outlet under different working conditions and α_{TE}.

5. Conclusions

In this paper, the aerodynamic performance and noise characteristics of a centrifugal air compressor for vehicle fuel cells were studied. The influence of α_{TE} on aerodynamic performance and flow characteristics was investigated by the CFD method. The effect of α_{TE} on aerodynamic noise excitation source and noise characteristics was studied by the FW–H equation and CFD–BEM coupling method. According to the results, the influence mechanism of different trailing edge sweep angles on flow characteristics and aerodynamic noise was revealed. The main conclusions were as follows:

1. The η_{is} of the impeller with TE sweep is improved under each operating condition. The higher the rotation speed, the greater the improvement. With the increase in the sweep angle, the variation of the η_{is} shows a trend of decreasing first and then increasing. Compared to the impeller without sweep, the peak η_{is} is improved by 0.26%, 0.62%, and 0.67%, respectively, for the three operating conditions with a sweep angle of 10°.
2. The α_{TE} affects the loss caused by the mixing of the tip clearance flow with the main flow, the flow separation loss at the tip near the TE pressure surface, and the flow separation loss at the TE of the middle blade height accordingly affects the efficiency of the impeller.
3. As the sweep angle increases, the acoustic dipole intensity distribution along the flow direction generally decreases. However, the larger the α_{TE} is, the larger the blade area near TE at the higher acoustic pole excitation intensity, which will affect the overall acoustic excitation intensity of the blade.
4. The *SPL* of the compressor under each working condition can be effectively reduced by the TE sweep. With the increase in α_{TE}, the *SPL* of aerodynamic noise decreases first, then increases, and then decreases due to the influence of impeller sound source intensity, position, and radiation area. The *SPL* is the lowest when the sweep angle is 15°. Compared with the impeller without TE sweep, when the α_{TE} is 15°, the *SPL* of the aerodynamic noise is reduced by 1.4 dBA under IC, 4.3 dBA under CC, and 5.8 dBA under HC. Therefore, the TE sweep has a significant effect on the reduction of aerodynamic noise. Considering the influence of α_{TE} on efficiency and aerodynamic noise, it is recommended that the α_{TE} of 10–15° be applied to impeller design.

Author Contributions: Investigation, S.S.; Methodology, S.S., M.Z. and W.C.; Project administration, Z.X.; Software, M.Z. and H.C.; Supervision, Z.X.; Validation, C.W. and H.C.; Writing—original draft, S.S. and Y.F.; Writing—review & editing, W.C. and C.W. All authors have read and agreed to the published version of the manuscript.

Funding: This research was funded by the National Key Research and Development Program of China, grant number 2019YFB1504604.

Data Availability Statement: Not applicable.

Acknowledgments: The support from Gree Electric Appliances Inc and HPC Platform, Xi'an Jiaotong University is appreciated.

Conflicts of Interest: The authors declare no conflict of interest.

Nomenclature

ρ	density
u, v, w	velocity
S	source term
T	temperature
c_p	specific heat at constant pressure
h	specific enthalpy
D	cross-diffusion term
PR	Pressure ratio
k	specific heat ratio
CFD	computational fluid dynamics
SST	shear stress transport
t	time
x, y, z	position coordinates
p	pressure
k	fluctuation kinetic energy
Γ	effective diffusivity
Y	dissipation term
ω	specific turbulence dissipation rate
η_{is}	isentropic efficiency
RANS	Reynold-averaged Naviers-Stokes
BEM	boundary element method

References

1. Raitor, T.; Neise, W. Sound generation in centrifugal compressors. *J. Sound Vib.* **2008**, *314*, 738–756. [CrossRef]
2. Fan, C. Simulation and Experimental Study on Aerodynamic Noise of Small Centrifugal Impeller. Master's Thesis, Harbin Engineering University, Harbin, China, 2021.
3. Sun, H.; Shin, H.; Lee, S. Analysis and optimization of aerodynamic noise in a centrifugal compressor. *J. Sound Vib.* **2006**, *289*, 999–1018. [CrossRef]
4. Zhang, F. Numerical Prediction Method and Experimental Analysis of Aerodynamic Noise of Marine Centrifugal. Master's Thesis, Jiangsu University of Science and Technology, Jiangsu, China, 2020.
5. Liu, C.; Zhang, W.; Cao, Y.; Pingjian, M.; Yang, L. Prediction of marine diesel turbocharger compressor aerodynamic noise at high efficiency operating conditions. *J. Harbin Eng. Univ.* **2019**, *4*, 8. [CrossRef]
6. Liu, C. Analysis of Aerodynamic Noise Characteristics of Centrifugal Compressor in a Marine Turbocharger. Ph.D. Thesis, Harbin Engineering University, Harbin, China, 2021.
7. Ganesh, C.S.; Nagpurwala, Q.H.; Dixit, C. Effect of Leading Edge Sweep on the Performance of a Centrifugal Compressor Impeller. *SASTech* **2011**, *9*, 55–62.
8. Zhao, H.; Wang, Z.; Tang, Y.; Xi, G. Effects of Blade Leading Edge Lean and Sweep on the Aerodynamic Performance of Centrifugal Impellers. *J. Xi'an Jiaotong Univ.* **2015**, *49*, 1–7. [CrossRef]
9. Guo, L.; Liu, Y.; Zheng, X.; Cui, Q. Effect of Hybrid Leading Edge Sweep on the Aerodynamic Performance of Small Scale Transonic Centrifugal Compressor. *Trans. CSICE* **2016**, *34*, 281–287. [CrossRef]
10. Wang, Y.; Liu, X.; Zhou, Y.; Fan, H.; Chen, Y.; Zhang, Z. Performance Analysis and Multi-Parameter Optimization of Centrifugal Impeller Configuration for the Centrifugal Compressor Used in Fuel Cell. *J. Xi'an Jiaotong Univ.* **2022**, *6*, 1–10.

11. Tian, H.; Tong, D.; Zhang, J.; Cheng, J.; Liu, X. Flow Characteristic of Transonic Centrifugal Compressor with Free-Form Sweep Impeller at Leading and Trailing Edges. *Trans. CSICE* **2021**, *39*, 554–560. [CrossRef]
12. Tian, H.; Tong, D.; Liu, Y.; Xing, W.; Chen, D.; Gao, C. The Effects of Blade Trailing Edge Swept on the Performance of Centrifugal Compressor. *J. Eng. Thermophys.* **2021**, *42*, 399–406.
13. Wu, H.; Huang, H.; Zhang, B.; Xiong, B.; Lin, K. CFD Simulation and Experimental Study of Working Process of Screw Refrigeration Compressor with R134a. *Energies* **2019**, *12*, 2054. [CrossRef]
14. Vycheslav, I.; Yuri, K.; Aleksei, D.; Yablokov, A.; Sokolov, M. Verification and Validation of CFD Modeling for Low-Flow-Coefficient Centrifugal Compressor Stages. *Energies* **2022**, *15*, 181. [CrossRef]